Photon correlation spectroscopy with high-energy coherent x rays

T. Thurn-Albrecht,[1,*] F. Zontone,[2] G. Grübel,[2] W. Steffen,[3] P. Müller-Buschbaum,[4] and A. Patkowski[5]
[1]*Physikalisches Institut, Albert-Ludwigs-Universität, Hermann-Herder-Strasse 3, 79104 Freiburg, Germany*
[2]*European Synchrotron Radiation Facility, Boîte Postale 220, 38043 Grenoble, France*
[3]*Max-Planck-Institute for Polymer Research, Ackermannweg 10, 55128 Mainz, Germany*
[4]*Physikdepartment, Technische Universität München, James-Franck-Straße 1, 85747 Garching, Germany*
[5]*Institute of Physics, A. Mickiewicz University, Umultowska 85, 61-614 Poznan, Poland*
(Received 31 March 2003; published 22 September 2003)

We performed x-ray photon correlation spectroscopy on a model suspension of colloidal particles using x rays of three different energies, namely, 8 keV, 13.5 keV, and 19 keV . The observed reduction in the degree of coherence with increasing x-ray energy, as measured by the contrast of the correlation functions, is consistent with theoretical estimates. We show that it is well possible and under certain circumstances even advantageous to perform experiments with coherent x rays at these higher energies. We argue that the reduced absorption may not only allow for thicker samples but also for longer acquisition times because of the reduced radiation damage, thus outweighing in many cases the effect of the reduced coherent flux. The use of higher energy x rays for photon correlation spectroscopy can therefore lead to a substantial increase in the signal-to-noise ratio and constitutes a promising option for future experiments on samples of polymeric or biological origin.

DOI: 10.1103/PhysRevE.68.031407 PACS number(s): 82.70.Dd, 05.40.Jc, 07.85.Qe, 42.25.Kb

I. INTRODUCTION

X-ray photon correlation spectroscopy (XPCS) is a relatively new technique made possible by the advent of third generation high brilliance synchrotron radiation sources. It allows one to measure slow dynamics on a small spatial scale in a scattering experiment. The technique has been used on a variety of colloidal and liquid crystal systems [1–6]. Applications to polymer systems [7,8] have been limited, partly due to severe problems with radiation damage caused by the high primary beam intensity necessary for the experiment [9]. Also, typically long acquisition times are needed. While it is known that radiation damage on organic samples can be reduced substantially by using higher energy radiation, such an approach has never been seriously explored for XPCS experiments, since in these experiments a coherent primary beam is needed and coherent flux from a synchrotron source scales with the square of the wavelength. It has rather been suggested recently that it is preferable to use soft x rays in order to increase coherent flux [4]. On the other hand the reduced absorption of higher energy x rays not only minimizes radiation damage and therefore allows for longer acquisition times, it also allows one to use thicker samples and to increase the scattering signal in this way. Here we show that XPCS experiments can indeed be performed with higher energy x rays. We observe a loss in the degree of coherence as expected, but this loss is generally weaker than the expected gain in the signal-to-noise ratio under circumstances where thick samples can be used.

II. THEORY

X-ray photon correlation spectroscopy is based on the same concept as the more commonly known dynamic light scattering technique [10] except for the use of coherent x rays. If a scattering experiment on a disordered sample is performed under highly coherent conditions the scattering pattern exhibits random interferences, so called ''speckles,'' which are not visible in a conventional scattering experiment due to incoherent averaging. The microscopic dynamics in the sample leads to fluctuations in the speckle pattern and the corresponding intensity fluctuations constitute the signal observed in photon correlation spectroscopy. The intensity fluctuations are quantified via the normalized intensity correlation function $g(q,t)$, with

$$g(q,t)=\frac{\langle n(q,0)n(q,t)\rangle}{\langle n(q,t)\rangle^2}=1+c(q)[f(q,t)]^2. \qquad (1)$$

Here $n(q,t)dt$ is the number of photons detected in time interval dt, q is the scattering vector and the brackets denote the ensemble average. $f(q,t)$ is the normalized intermediate scattering function, which is related via Fourier transform to the dynamic structure factor. Equation (1) holds for a homodyne experiment, and Gaussian statistics for the scattered field is assumed. Photon correlation spectroscopy is therefore equivalent to a quasielastic scattering experiment, but it offers access to the dynamics on a much longer time scale. As mentioned above, the intensity fluctuations giving rise to $g(q,t)$ can only be observed with coherent light. It is required that the radiation impinging on the detector from any point in the sample and at any time can interfere. Under these conditions $c(q)$, the so called contrast of the correlation function, is equal to unity. In a real experiment usually only partially coherent illumination is achieved, then $c(q)<1$ [10]. The coherence conditions required for such an experiment can be estimated as follows [11,12].

(1) The maximum path length difference of two photons scattered in the sample has to be smaller than the longitudinal coherence length $\xi_l=\lambda^2/\Delta\lambda$. On a typical synchrotron

*Present address: Martin-Luther-University Halle-Wittenberg, Physics Department, 06099 Halle, Germany.

beam line equipped with a standard silicon monochromator ($\Delta\lambda/\lambda \simeq 10^{-4}$) this condition is always fulfilled in the so called small-angle scattering regime ($q \lesssim 0.1$ Å^{-1}, $\lambda \approx 1.5$ Å).

(2) In order to ensure spatial coherence of the incoming beam a pinhole has to be used in front of the sample, whose size L is comparable to the transverse coherence length ξ_t:

$$L \simeq \xi_t = \frac{\lambda R}{2 d_s}. \tag{2}$$

Here R is the distance from the source and d_s the size of the source. For the typical parameters of a synchrotron beam line ($R \approx 60$ m, $d_s \approx 200$ μm) ξ_t amounts to about 20 μm for radiation with $\lambda \approx 1.5$ Å.

(3) The speckles showing up in an experiment performed under these conditions will have a typical width (solid angle) $\Delta\Omega \simeq (\lambda/L)^2$. To detect them the detector area A has to be comparable to the size of a speckle:

$$A \approx r^2 \left(\frac{\lambda}{L}\right)^2. \tag{3}$$

Here r denotes the distance between the sample and the detector.

The prefactors used in the relations above depend of course on the exact criterion used for the visibility of the speckles, but independently some relations concerning the use of radiation with varying wavelength λ can be obtained. If λ is varied and the pinhole in front of the sample is changed according to Eq. (2), the intensity usable in the experiment will scale with wavelength as λ^2. A variation of λ alone (without adjusting the size of the incident pinhole) has a similar effect as a varying detector size. If the area of the detector is increased beyond the value given in Eq. (3) the observed amplitude of the intensity fluctuations will decrease. For large detector areas the following relation holds [10]:

$$c(q) \sim \frac{(\lambda/L)^2}{A/r^2}. \tag{4}$$

Equation (4) also shows that in an experiment with varying wavelength the contrast of the correlation function will be in a first approximation proportional to λ^2.

On the other hand, using x rays with a higher energy E_x allows one to choose a thicker sample. For a given absorption coefficient μ, the scattering signal is optimized for a sample thickness $d \approx 1/\mu$. Apart from abrupt changes at absorption edges, μ varies as λ^3, and a gain in the number n of scattered photons, $n \sim \lambda^{-3}$, can be achieved. In addition, radiation damage is reduced. If we assume that radiation damage is simply proportional to the energy transfer given by $\mu E_x \propto \lambda^3 \lambda^{-1} = \lambda^2$, the possible time of acquisition T for constant radiation damage scales as λ^{-2}. The quantity which determines the statistical quality of a measured correlation function at low count rates is the relative statistical error with which the contrast, i.e., the value of $g(q,t)$ for $t \ll \tau$, can be determined. τ stands here for the typical time scale on which the correlation function decays to one. In this limit, the correlator $\langle n(q,0)n(q,t)\rangle$ behaves like a Poisson variable [13], i.e., $\Delta\langle n(q,0)n(q,t)\rangle = \sqrt{\langle n(q,0)n(q,t)\rangle}$. This results in

$$\Delta g(t) = \sqrt{g(t)} \frac{1}{\langle n \rangle \sqrt{T \Delta t}} \tag{5}$$

for the correlation function defined in Eq. (1). T denotes the total time of the measurement and Δt is the time interval used to measure $n(t)$, which for the correlator used (ALV, Langen, Germany) depends on the argument t. The number of sampling intervals M is given by $T/\Delta t$ and $\Delta g \sim 1/\sqrt{M}$. Consequently, using a sample with optimum thickness and allowing for maximal time of measurement, $\langle n \rangle \sim \lambda^{-3}$ and $T \sim \lambda^{-2}$, resulting in

$$\Delta g(t) \sim \frac{1}{\lambda^{-3}\sqrt{\lambda^{-2}}} \sim \lambda^4. \tag{6}$$

Here we used the fact that the scattering cross section is independent of λ and an energy independent flux of photons in the primary beam was assumed. Additional effects might come into play by absorption induced heating, which might make an experiment completely impossible if absorption is too high. Altogether we can conclude that by using optimized conditions the statistical accuracy in an XPCS experiment can indeed increase if higher energy photons are used, since $\Delta g(t)$ decreases more strongly with decreasing λ than the contrast given in Eq. (4), i.e.,

$$\frac{\Delta g(t)}{c(q)} \sim \frac{\lambda^4}{\lambda^2} \sim \lambda^2. \tag{7}$$

Given that due to the experimental conditions described above, XPCS experiments are usually intensity limited and therefore limited by statistical accuracy, the use of higher energy x rays can be a very relevant option. The feasibility of this option is demonstrated here.

III. SAMPLE

Silica particles with a nominal radius $R = 290$ nm suspended in water (10% weight) were purchased from Microparticles, Berlin, Germany. The size of the particles was checked with dynamic light scattering, giving a hydrodynamic radius $R_h \approx 255$ nm (extrapolated value for concentration $\phi \to 0$). For the XPCS experiments, the particle suspension was diluted with glycerol in order to increase the viscosity of the solution. Three volume parts glycerol were added to one volume part water based suspension resulting in a volume fraction of 1.1% of the silica particles in the sample. Here we assumed a density of 2.5 g cm^{-3} for the silica particles. By adding glycerol the time scale of diffusive motion is shifted to a range more convenient for the experiment (about two orders of magnitude slower). The colloidal suspension was filled in glass tubes with a diameter of 1.5 mm (8 keV measurements), 5 mm (13 and 19 keV measurements), or 10 mm (19 keV measurements). The transmission

TABLE I. Measured transmission for samples of different thickness (left column) and different x-ray energies (top row). The values are corrected for absorption by the container walls.

Diameter(mm)	8 keV	13.5 keV	19 keV
1.5	0.20		
5		0.39	0.69
10			0.39

of the samples after correction for the glass wall of the capillary (not all identical) is shown in Table I.

IV. EXPERIMENTAL SECTION

The experiment was performed at the Troika III station of the Troika beam line ID10A at the European Synchrotron Radiation Facility (ESRF) [14]. A schematic view of the setup is shown in Fig. 1. The synchrotron was running in 16-bunch mode with an average current of about 70 mA. The Troika beam line uses three undulator sources: two standard ESRF undulators and one short small-gap undulator, all installed in a high-β straight section. Measurements were performed at the third (7.990 keV), fifth (13.476 keV), and seventh (18.984 keV) harmonic of the standard undulators, the small-gap undulator having the first harmonic always tuned at 7.99 keV. The source size of the ESRF high-β sections is typically about 930 μm (horizontal) and 25 μm (vertical) full width at half maximum. We used a slit to reduce the apparent horizontal size to about 200 μm in order to increase the transverse coherence length in the horizontal plane. The beam is monochromatized by a double bounce channel-cut Si(111) monochromator diffracting in the horizontal plane and located 59.5 m from the source. To suppress higher harmonics the second crystal is slightly detuned by a piezoelectric actuator. The coherent beam is provided by a 20 μm pinhole placed 25 cm upstream from the sample. A pair of slits located 45 cm further upstream can be used to precollimate the beam in front of the pinhole. Keeping these slits tight leads to a substantial increase in coherence, i.e., contrast of the correlation function. With this setup the primary beam intensity was 7.3×10^6 photons/(s mA) at 8 keV, 6.2×10^6 photons/(s mA) at 13.5 keV, and 3.4×10^6 photons/(s mA) at 19 keV. The sample is mounted in an evacuated small-angle scattering chamber and the scattered photons are guided through a vacuum flight path to the detector stage, giving a sample-to-detector distance of 2.3 m. Photons are detected by a Bicron scintillation counter equipped with an adjustable pair of slits, typically set to 20 $\times 20$ μm. Correlation functions are calculated in real time with an ALV 5000 correlator.

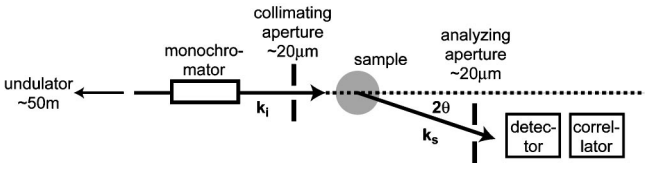

FIG. 1. Schematic of the experimental setup used on Troika III for coherent scattering experiments.

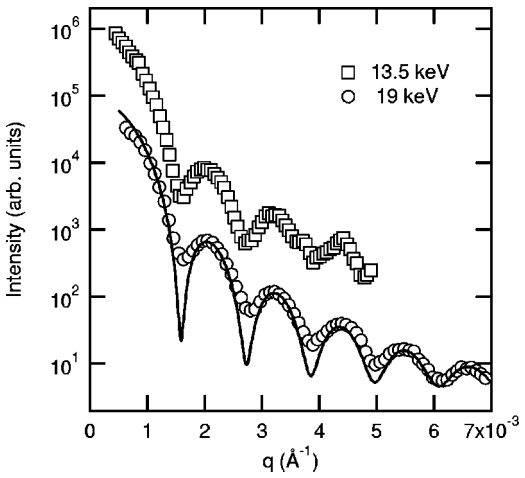

FIG. 2. Intensity vs scattering vector q of colloidal silica in suspension, measured at two different x-ray energies as indicated (second dataset shifted). The line corresponds to a model function for a polydisperse collection of spheres with an average radius of 283 nm ($\sigma=6.3$ nm). Measurements were performed under the same conditions as the photon correlation spectroscopy experiments.

V. RESULTS AND DISCUSSION

Figure 2 shows the measured scattering intensity of the colloidal silica suspension at x-ray energies of 19 and 13.5 keV as a function of the scattering vector q. The pronounced oscillations are due to the particle form factor. Because of the dilute state of the suspension no interference effects are observed, the structure factor being equal to unity. For comparison, model data calculated for a polydisperse ensemble of spheres with an average radius $R=283$ nm and a standard deviation $\sigma=6.3$ nm are shown (Gaussian distribution assumed). The discrepancies between the model and the data are related to the momentum resolution not taken into account. While the divergence of the primary beam is of course extremely small, the finite momentum resolution is caused by the finite size of the detector slits. The dynamic measurements were performed in the range of low q up to about the second minimum around $q=2.7\times10^{-3}$ Å^{-1}.

Three exemplary correlation functions measured at different x-ray energies for an equivalent scattering vector $q\approx7.6\times10^{-4}$ Å^{-1} are shown in Fig. 3. As expected we observe a strong change in contrast while the time scale on which the correlation functions decay remains unchanged. For simple translational diffusion the correlation function measured in a homodyne experiment can be described by an exponential function

$$g(t)=c(q,\lambda)\exp(-2\Gamma t)+1 \quad \text{with} \quad \Gamma=Dq^2. \tag{8}$$

Here $c(q,\lambda)$ is the contrast of the correlation function and D the diffusion constant, which in the dilute limit is given by the Stokes-Einstein relation $D=kT/6\pi\eta R_h$. R_h denotes the hydrodynamic radius of the particles and η the viscosity of

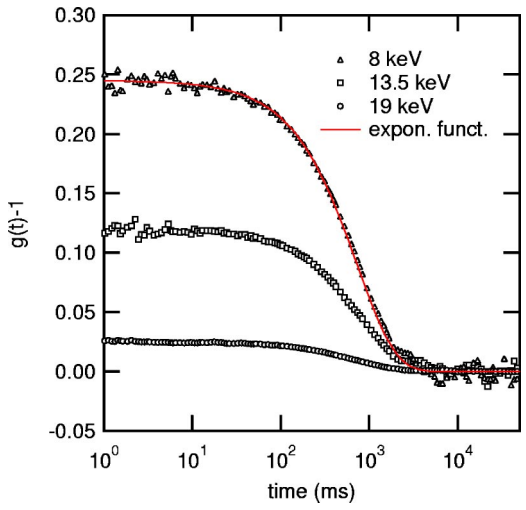

FIG. 3. (Color online) Exemplary correlation functions of colloidal silica suspension measured at $q \approx 7.6 \times 10^{-4}$ Å^{-1} using three different x-ray energies as indicated. Identical collimation conditions were used (20 μm pinhole and 20 μm detector slits). The contrast of the correlation functions depends strongly on the x-ray energy used. For the dataset measured at 8 keV the model function (simple exponential) resulting from a fit with Eq. (8) is shown as a continuous line.

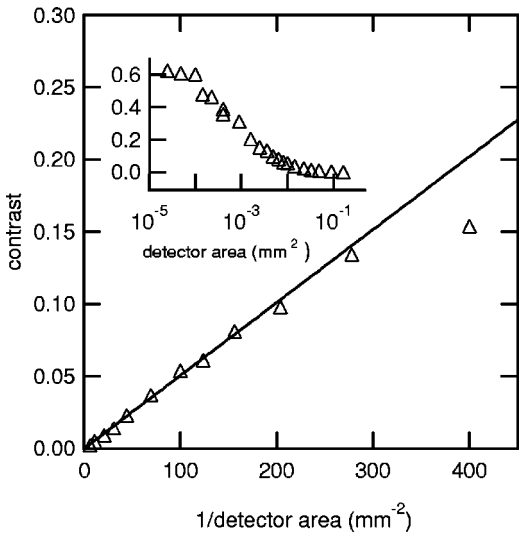

FIG. 5. Contrast c of correlation function as determined from a series of measurements with varying detector area A, measured at $q = 7.58 \times 10^{-4}$ Å^{-1} and x-ray energy $E_x = 8$ keV. The straight line corresponds to the behavior expected for $A \gg (r\lambda/L)^2$. The inset shows the full set of data presented on a semilogarithmic scale. Note the large value of the contrast obtained for very small detector openings.

the solvent. For a heterodyne experiment, i.e., if the scattered intensity is mixed coherently with statically scattered intensity, the factor of 2 in the exponent would disappear. The fact that we measure the same values for Γ at all energies with different static background contributions confirms that the experiment is always performed in the homodyne regime. A series of correlation functions was measured at each of the three x-ray energies; the resulting values for $\Gamma(q)$ are shown in Fig. 4. As expected, the data show a common q^2 dependence, measurements taken at different energies are fully consistent.

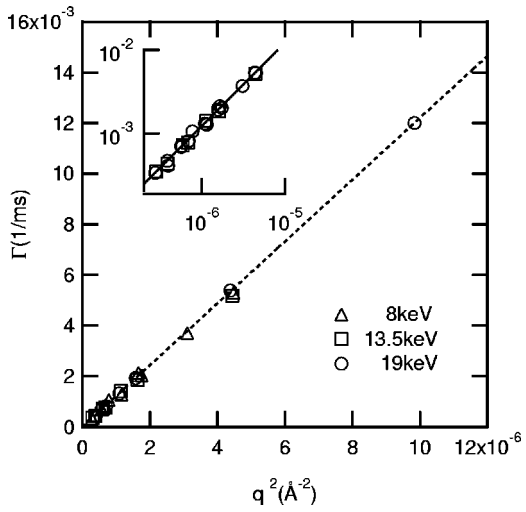

FIG. 4. Decay rate Γ of correlation function vs the square of the scattering vector q, measured with x rays of different energies as indicated. The data show that the diffusion constant can be measured consistently, independent of the x-ray energy used. The inset showing the same data on a log-log-scale proves that indeed $\Gamma \propto q^2$ over the full range of scattering vectors used.

Let us now turn to the discussion of the coherence properties encountered in the experiment. As described above by Eq. (4) for our experiment a variation of the x-ray wavelength has in first approximation the same effect as a variation of the detector size while keeping the wavelength constant. We therefore performed a series of measurements taken with varying detector size at a given scattering vector $q = 7.58 \times 10^{-4}$ Å^{-1}. The contrast c of the correlation function as a function of detector area A is shown in the inset of Fig. 5 over a large range of A. The contrast decreases with increasing detector size, in the limit of large A as $1/A$, as can be seen in the main part of Fig. 5. For small A the contrast levels off because here the detector area is comparable or smaller than the size of a speckle, $(r\lambda/L)^2 \approx 3 \times 10^{-4}$ mm^2 on the detector (see inset of Fig. 5).

Keeping the detector area constant we can observe changes in coherence properties by determining the contrast from a series of measurements taken with different x-ray energies. The result is shown in Fig. 6. The data points scatter relatively strongly, especially at low q. The reason is most likely some static background contribution due to scattering from the pinhole which varies from measurement to measurement. This contribution is stronger at low q and even with careful alignment it is difficult to remove it completely. Nevertheless the data clearly correspond to the expectations formulated above in Eq. (4), i.e., the contrast decreases with increasing x-ray energy. For a semiquantitative analysis we start from the data taken at the highest energy, since in this case a limiting value for $c(q)$ at high q can be determined unambiguously, as indicated by the horizontal line. The two dotted lines show the expected contrast for the other energies

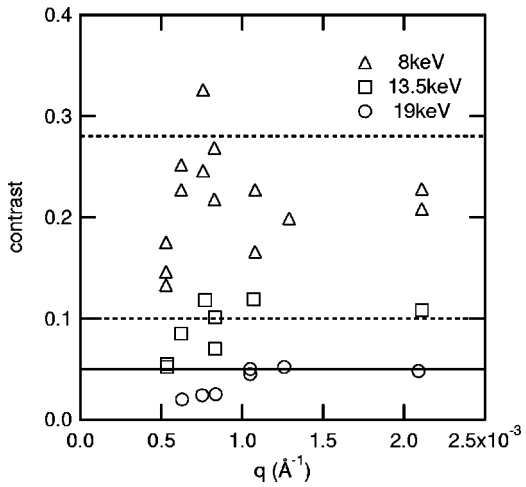

FIG. 6. Contrast c of correlation function vs scattering vector q as determined from a series of measurements taken with different x-ray energies as indicated. Collimation conditions as above were used (20 μm pinhole and 20 μm detector slits). The dotted lines indicate the expected value of the contrast based on a λ^2 scaling of the value determined for $E_x = 19$ keV. The estimated values are consistent with the data, although there are deviations, which are most likely caused by static background signal originating from pinhole scattering.

based on a scaling with λ^2. While the data points determined from the measurements at 13 keV agree reasonably well with this prediction, for most measurements at 8 keV this contrast could not be reached. This is most likely due to the background originating from scattering at the pinhole, which plays a more significant role for a thinner sample as it is used for the measurements taken at 8 keV. The fact that the loss of coherence at higher energies is not larger than estimated in Sec. II means that the arguments given there concerning the statistics of XPCS measurements are indeed valid.

VI. CONCLUSIONS

Our data clearly show that it is feasible to perform XPCS experiments with higher x-ray energies than used in previous experiments. If thicker samples can be used, higher energy x rays offer advantages, since due to reduced absorption there can be a net gain in signal. The use of higher energy x rays constitutes therefore a promising option for future experiments especially on polymeric and biological sample systems. We are convinced that the dynamics of these kind of systems which are able to form soft, self-assembled structures on a size scale of nanometers are most interesting to explore in future experiments using the XPCS technique. The use of higher energy radiation can also be useful for hard-condensed matter systems where the bulk sensitivity can be greatly enhanced by the large penetration depth.

ACKNOWLEDGMENTS

We are grateful to Florian Ebert for his help during the experiment and to A. Wilk for the light scattering measurements. We thank Henri Gleyzolle and Patrick Feder for technical assistance. Financial support by the German Federal Ministry of Education and Research (BMBF Contract No. 03TAE3FR) is gratefully acknowledged.

[1] S. Dierker, R. Pindak, R. Fleming, I. Robinson, and L. Berman, Phys. Rev. Lett. **75**, 449 (1995).
[2] T. Thurn-Albrecht, W. Steffen, A. Patkowski, G. Meier, E. Fischer, G. Grübel, and D.L. Abernathy, Phys. Rev. Lett. **77**, 5437 (1996).
[3] G. Grübel, D.L. Abernathy, D.O. Riese, W.L. Vos, and G.H. Wegdam, J. Appl. Crystallogr. **33**, 424 (2000).
[4] A.C. Price, L.B. Sorensen, S.D. Kevan, J. Toner, A. Poniewierski, and R. Holyst, Phys. Rev. Lett. **82**, 755 (1999).
[5] A. Fera, I. Dolbnya, G. Grübel, H.G. Muller, B.I. Ostrovskii, A.N. Shalaginov, and W.H. de Jeu, Phys. Rev. Lett. **85**, 2316 (2000).
[6] A. Madsen, J. Als-Nielsen, and G. Grübel, Phys. Rev. Lett. **90**, 085701 (2003).
[7] S.G.J. Mochrie, A.M. Mayes, A.R. Sandy, M. Sutton, S. Brauer, G.B. Stephenson, D.L. Abernathy, and G. Grübel, Phys. Rev. Lett. **78**, 1275 (1997).
[8] D. Lumma, M.A. Borthwick, P. Falus, L.B. Lurio, and S.G.J. Mochrie, Phys. Rev. Lett. **86**, 2042 (2001).
[9] V. Cherezov, M. Caffrey, and O. Diat, Biophys. J. **80**, 1225 (2001).
[10] B. Berne and R. Pecora, *Dynamic Light Scattering* (Wiley-Interscience, New York, 1975).
[11] J. Als-Nielsen and D. McMorrow, *Elements of Modern X-Ray Physics* (Wiley, Chichester, 2001).
[12] B. Lengeler, Naturwissenschaften **88**, 249 (2001).
[13] K. Schätzel, in *Dynamic Light Scattering*, edited by W. Brown (Clarendon Press, Oxford, 1993).
[14] G. Grübel, J. Als-Nielsen, and A. Freund, J. Phys. IV **4**, C9/27 (1994).